A Laboratory Experiment on the Dynamics of the Land and Sea Breeze

SHIGEKI MITSUMOTO AND HIROMASA UEDA

National Institute for Environmental Studies, Tsukuba, Ibaraki 305, Japan

HIROYUKI OZOE

School of Engineering, Okayama University, Okayama 700, Japan

(Manuscript received 25 May 1982, in final form 7 January 1983)

ABSTRACT

The land and sea breeze (LSB) circulation was simulated in a laboratory using a temperature controlled water tank. Flow visualization by tellurium and phenolphthalein and velocity measurement by laser-Doppler velocimeter were carried out in addition to temperature measurements. From similarity considerations, the simulated flow pattern was shown to have good correspondence with that in the atmosphere. It was shown that the overall features of the LSB flow pattern consist of a closed circulating motion caused by the periodically changing horizontal temperature difference between the land and the sea, and several kinds of small-scale motions induced by the periodic variation of the land surface temperature itself. The most important small-scale motion is the cellular convection which occurs all over the land surface due to unsteady heating from below in the morning calm. Other small-scale motions, such as longitudinal vortex rows which are formed inland throughout the sea breeze layer, and gravity currents, were also investigated and shown to contribute significantly to the dynamics of the LSB and the transport of a pollutant within it.

1. Introduction

The land and sea breeze (LSB) circulation is a typical local wind with diurnal period. Recently, much attention has been focused on it as a problem of pollution-related meteorology because an emitted pollutant accumulates in the atmosphere due to the closed LSB circulation (Anthes and Warner, 1978; Kondo and Gambo, 1979; Ozoe *et al.*, 1983). From the viewpoint of transport phenomena, the LSB is of great interest since it is composed of important physical mechanisms which have not yet been investigated, such as unsteady natural convection, gravity current, stratification effects on the transport processes (Ueda *et al.*, 1981), etc. It was first studied using linear analysis by Jeffreys (1922), and Haurwitz (1941, 1947). These theoretical works and the field measurements up to that time were summarized by Wexler (1946), and Defant (1951).

In order to make clear the effects of the nonlinear terms involved in the set of governing equations, Estoque (1961) first studied the LSB using a two-dimensional numerical model. His work was followed by many meteorologists. Later, the interaction with the gradient wind (Estoque, 1962), the effects of a curved coastline using a three-dimensional model (McPherson, 1970), and the orographical effects of a slope (Mahrer and Pielke, 1977; Asai and Mitsumoto, 1978) were investigated using numerical experiments. It has been confirmed that these numerical models can simulate the general features of the LSB, and so they are being used for atmospheric simulation for actual regions (Anthes and Warner, 1978; Kikuchi *et al.*, 1981).

On the other hand, many field observations of land and sea (or lake) breeze have been carried out, among which the observations at Lake Michigan (Lyons and Olsson, 1973; Keen and Lyons, 1978) illustrate the actual land and sea/lake breeze as a mesoscale phenomenon. These numerical investigations and field observations together have elucidated the overall feature of the LSB.

Keen and Lyons (1978) noted the importance of the thermal internal boundary layer in their field measurements, and they, as well as Simpson and Britter (1980) in their laboratory experiment, pointed out the important role of vertical motion at the sea-breeze front on the transport of pollutants. The scales of these physical mechanisms are small compared with the whole flow field of the LSB and so they have not been taken into sufficient account in the theoretical models. Therefore, it is important at this stage to clarify what kinds of physical mechanisms contribute to the land and sea breeze phenomenon and how they contribute to the overall features of the LSB.

The purpose of this paper is to make clear in a laboratory experiment the fundamental physical mechanisms involved in the LSB. A specially-designed water tank was used to simulate the LSB. The structure of the LSB circulation, as well as the small-

scale motions and their time changes were observed. The advection and diffusion of material in the flow were also investigated.

2. Experimental apparatus

The test fluid, fresh water was put into a Plexiglas water tank, 2000 mm wide × 600 mm wide × 400 mm tall, to a depth of 100 mm (Fig. 1). Two equally-sized water jackets made of 1 mm thick stainless steel were horizontally submerged side by side at the bottom of the tank. The temperature of the water circulating through the right-hand-side bottom jacket ("LAND" in Fig. 1) was controlled by the combination of an electric heater (15 kw), PID (Proportional, Integral, Differential) controller, arbitrary function generator and resistance thermometer. The temperature at the entrance of the bottom jacket was compared with the signal generated by the arbitrary function generator, and the electric current to the heater was controlled by the PID feedback system, so that the temperature varied sinusoidally with constant amplitude and period. In the present experiment, the amplitude and period were chosen to be 1.6 K and 12 min, respectively, with a time-averaged temperature of 303 K. The temperature of the left-hand side bottom jacket ("SEA" in Fig. 1) was kept constant (303 K) throughout the experimental runs. These jackets were carefully designed so that their surface temperature stays uniform and they respond quickly to the variation of the temperature of the circulating water.

The upper surface of the test fluid was covered by another water jacket made of 1 mm thick stainless steel (SKY in Fig. 1) through which water at constant temperature 313 K (10 K warmer than the SEA) circulated. This jacket was replaced with a water jacket made of Plexiglas plates to provide flow visualization from above. The plexiglas plate is not a good heat conductor but is good enough to maintain a uniform upper surface temperature, if the simulated fluid motion of the LSB is limited to the lower layer of the test fluid. Thus, the test fluid was basically stably stratified with a linear temperature profile. The bottom jackets at the left- and right-hand sides were regarded as SEA and LAND, respectively, the border line between them being regarded as the COASTLINE.

The choice of experimental conditions, which will be discussed in Section 5a, was found adequate to confine the flow region of the simulated LSB to the lower layer of the test fluid, and the x-length of the water tank was enough so that fluid motion was not significantly affected by the end walls. Here, x-y-z coordinates are defined as follows: 1) the x axis is horizontal, perpendicular to the COASTLINE, $x > 0$ on the land side; 2) the y axis is along the COASTLINE; and 3) the z axis is vertical, $z > 0$ upward. The aspect ratio (height to the y-width) of

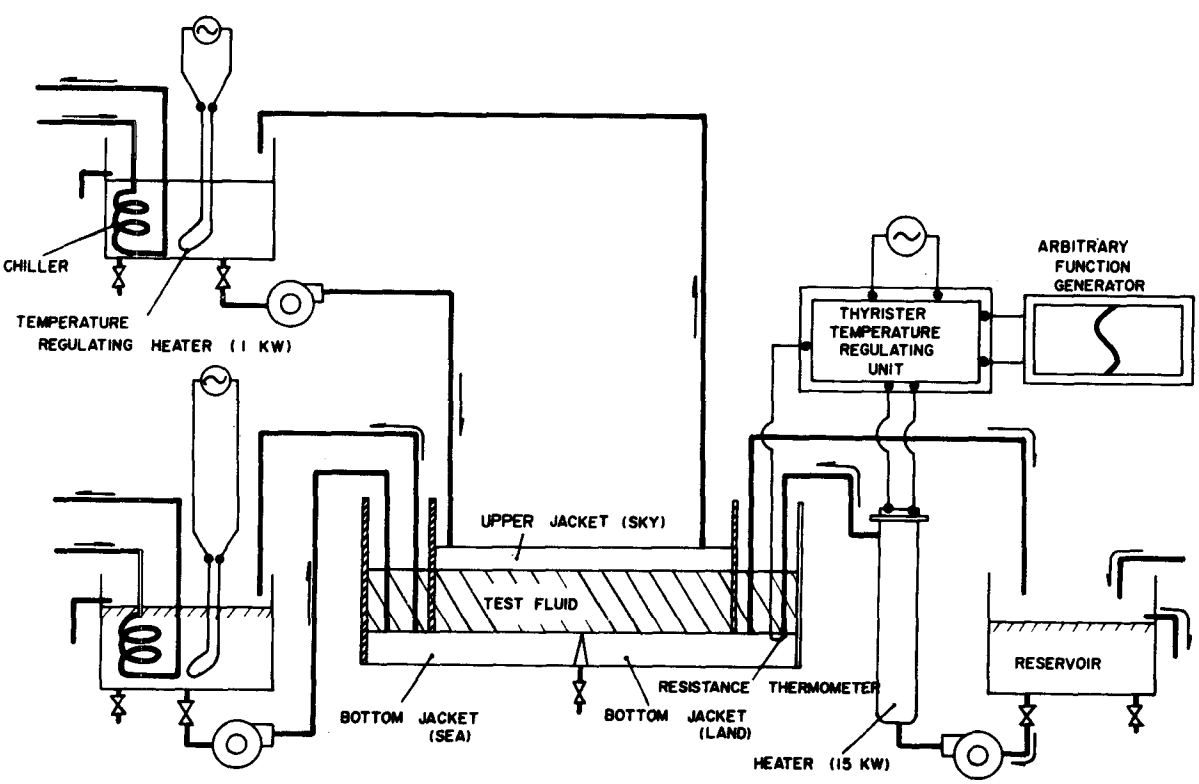

FIG. 1. Schematic diagram of experimental apparatus.

the test fluid region is 1/6, sufficiently small to keep the flow two-dimensional. As a preliminary experiment, the y-distribution of flow velocity in the x-direction was measured. It was found that the flow was free from effects of the side walls in the region -10 cm $< y < +10$ cm, so that in this region the overall feature of the flow can be regarded as two-dimensional. The subsequent descriptions of the mean flow is limited to the x-z plane at $y = 0$.

3. Experimental procedure

After the aforementioned conditions were maintained for several hours, the fluid motion became sufficiently periodic. Then, the flow was visualized by two methods; 1) tellurium electrolyte method and 2) phenolphthalein electrolyte coloration method. After several circulation periods, the flow was photographed with a 35 mm still camera and 16 mm movie camera by slow-speed filming.

a. Tellurium electrolyte method

A small lump ($\sim$3 mm in diameter) of tellurium metal was suspended by a fine copper wire $\sim$50 mm above the coastline, and served as a cathode. When 5–10 V DC was applied between the tellurium and the bottom jackets, the tellurium electrolyte was emitted as a black smoke. The smoke was a good tracer for the slowly moving flow because the settling speed of the smoke particles was less than 0.1 mm s^{-1}.

b. Phenolphthalein electrolyte coloration method

Visualization using tellurium was limited to the observation of the flow mode in the two-dimensional, vertical cross-section. In order to observe the three-dimensional structure of the convection, which will be mentioned later, the phenolphthalein electrolyte coloration method was employed.

By adding small amounts of NaOH and HCl to the test fluid, it was made slightly alkaline just before the phenolphthalein (0.1 g per liter) contained in the test fluid was colorized. The surface of the bottom jackets worked as a cathode, and a net of copper wire suspended within the test fluid near the upper jacket as an anode. When a direct current of $\sim$10 V was applied between them, a red color was generated in the thin layer all over the land and sea surfaces, enabling the visualization of the three-dimensional convective pattern.

c. Velocity and temperature measurements

Vertical distribution and time variations of the horizontal velocity u (perpendicular to the coastline), vertical velocity w, and temperature T were measured at several sections above the sea, coastline and the land.

For the measurement of very low velocity, a laser-Doppler velocimeter (DISA Type 55X series) was used. By means of polarization separation, simultaneous measurement of two velocity components was made in the differential Doppler mode with a monocolor (He-Ne) laser. The split laser beams passed through a Plexiglas front wall and were focused on the center line of the test tank by a 600 mm focal length lens. The scattered light was collected by a photomultiplier through the back wall. The beam intersection point was moved vertically and laterally by a traversing mechanism.

Temperature measurement was obtained by means of a sheathed Ni-NiCr thermocouple 0.25 mm in diameter. It traversed vertically in 30 s, which was a short time compared with 12 min, the period of the LSB circulation. Disturbance of the flow and temperature fields due to the thermocouple traverse was negligible, and the thermocouple response to the temperature change was checked in the preliminary test to be rapid enough to detect the thermal structure related to the LSB.

4. Results

a. Visualized flow patterns

Characteristics of the flow observed by the flow visualization techniques will be presented according to the time change of the land surface temperature T_{LAND}. The photographs shown in Fig. 2 were taken after emitting tellurium for several periods. At "time 1", when the land surface temperature T_{LAND} equalled the sea surface temperature T_{SEA}, the "land breeze" was still dominant. Approximately 1.5 min later ("time 2"), small convective cells suddenly broke out all over the land surface, carrying the black smoke, which had been hovering near the land surface, upward. This cellular convection developed up to a height of $\sim$2–3 cm from the bottom, forming a uniformly thick mixed layer over the land. After this sudden occurrence of cellular convection settled ("time 3"), the "sea breeze" intruded over the land swirling counterclockwise in the x-z plane. The head of the sea breeze was accompanied by strong upward motion at its leading edge. Photo 4 (Fig. 2) shows the intrusion of the sea breeze deep over land. The sea breeze was accompanied by compensating flow at the height of 3 cm. The compensating flow aloft was also recognized in the land breeze phase, as seen in Photo 1. Photo 5 shows the weakening of the sea breeze as T_{LAND} decreases to its minimum and its change to a land breeze. Cellular convection does not occur at this stage.

In order to observe the three-dimensional structure of the convective motions, phenolphthalein was colorized all over the bottom surface.

Fig. 3a, corresponding to the same stage in Photo 2 of Fig. 2, shows a Bénard-type cellular convection

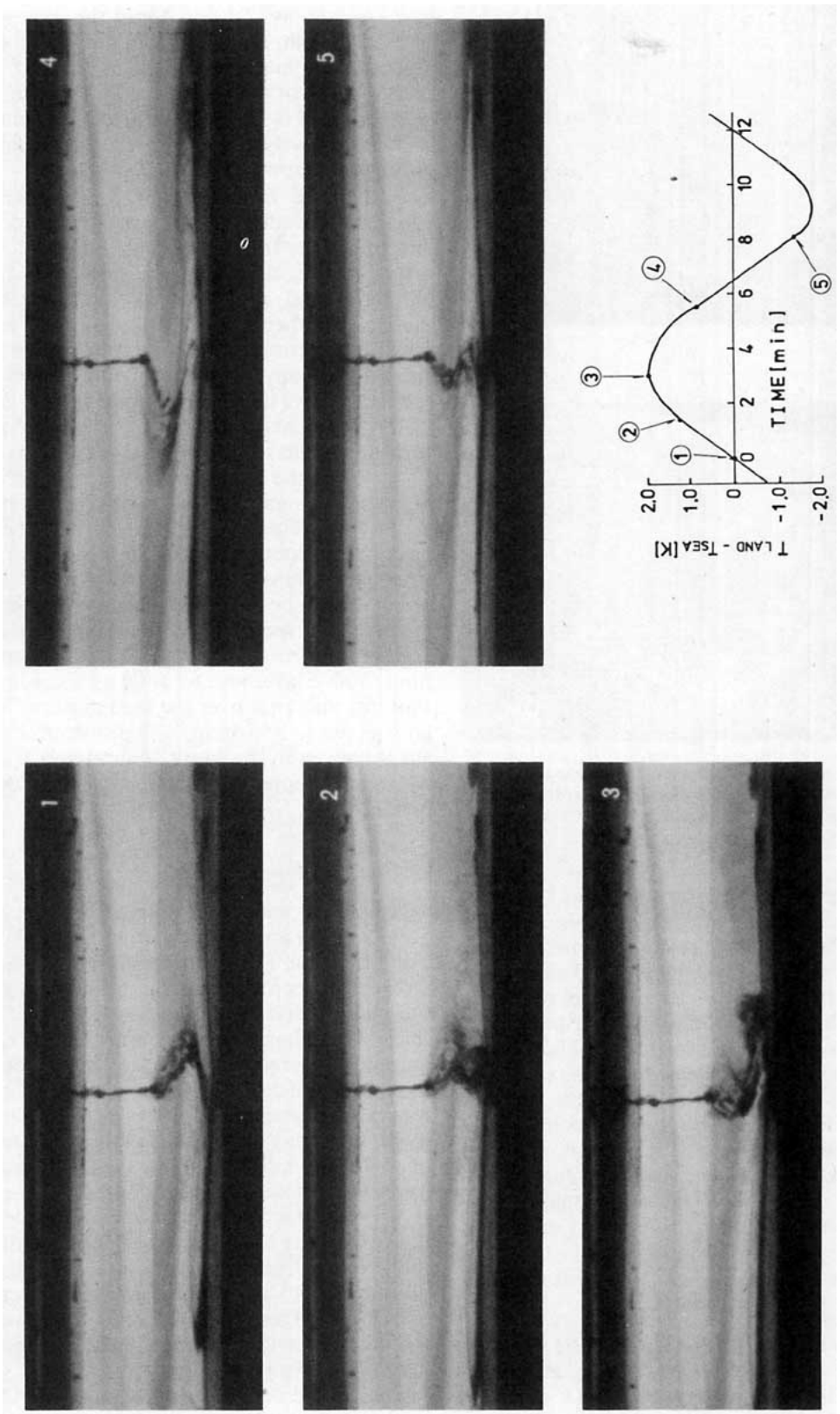

FIG. 2. Flow pattern visualized by tellurium method. The temperature of land surface T_{LAND}, corresponding to each pattern is shown.

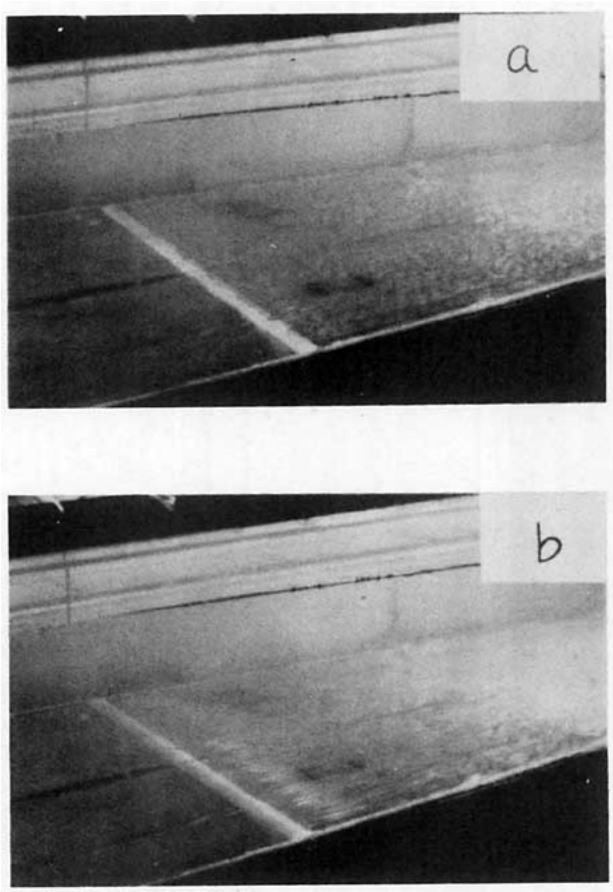

FIG. 3. Three-dimensional structure of flow near the surface visualized by phenolphthalein coloration: (a) Bénard convection over the land surface and (b) longitudinal vortex rows accompanying the intrusion of sea breeze.

occurring uniformly over the land surface. The mean diameter of each cell is ~2 cm, approximately the same as its height. When the sea breeze intrudes over land (Fig. 3b, corresponding to photo 3 of Fig. 2), longitudinal stripes are found over the region in which the sea breeze intruded. These stripes are attributed to the occurrence of longitudinal convective vortices with their axes parallel with the x-axis. When the sea breeze is replaced by the land breeze, the land breeze penetrates underneath the phenolphthalein layer over the sea surface, and, as a result, produces a prominent leading edge without disturbing the surrounding fluid on the sea. This wedge-shaped land breeze front can be identified as a gravity current.

b. Distributions of velocity and temperature

Some examples of the time variations of u, w and T are shown in Figs. 4–6, together with the variation of temperature difference, $T_{\mathrm{LAND}} - T_{\mathrm{SEA}}$ as a reference. In the entire region above the sea ($x < 0$), and in the upper layer over land ($z > 20$ mm, $x > 0$), u, w and T vary along a sine curve with the same 12 min period as T_{LAND}. Near the sea surface at $x = -170$ mm, the maximum sea breeze occurs 2.5 min after the maximum T_{LAND} is attained. The maximum speed of the sea breeze and land breeze were accompanied by the minimum and maximum values of w respectively. The phases of u, w and T advance as one goes upward.

In the lower layer over land ($z < 20$ mm, $x > 0$), the same periodic variations are observed, but their shapes deviate from a sine curve, that is, ~1.5 min after T_{LAND} exceeds T_{SEA}, a perturbation with a much shorter period is superimposed on the basic sine curve. This phenomenon, which is most evident for w, is characteristic of the land side. This is caused by the cellular convection described in Section 4a.

Fig. 7 shows the vertical profile of u at each phase of the time variation of T_{LAND}. Here, the phase ϕ is measured from the moment at which T_{LAND} exceeds T_{SEA}. When the sea breeze or land breeze is well developed, a reverse of the flow direction is noted near $z = 1.5$ cm. The breeze generated near the coastline at $\phi = \pi/2$ extends toward both land and sea, until it prevails over a wide region at $\phi = \pi$.

Fig. 7 also shows the vertical profile of temperature at each corresponding phase. At $\phi = \pi/2$, cellular convection prevails over the land side, eroding the upper stable layer and forming a mixed layer with a uniform thickness over the land surface. The mixed layer grows to $z = 3$ cm. The profile of T at $x = -1$ cm is convex in the lower layer at $\phi = 0$ and $3\pi/2$, which is attributed to the advection of the colder land breeze.

c. Detailed flow pattern

Amplitude and phase difference of the basic time variation of u are compared among each vertical section in Fig. 8a. Here, amplitude is defined as the difference between the maximum and minimum, and the phase difference as the phase delay of the minimum of u compared to the minimum of T_{LAND}. The amplitude is greatest at $z = 0.5$ cm and decreases to a minimum at $z = \sim 1.5$–2.0 cm at each section. This minimum corresponds to the interface between the main flow and compensating flow. Note that the height of the interface above the coastline is slightly lower than those inland and offshore. The phase delays almost linearly with height above the land and the sea. In the lowest layer adjacent to the surface, the phase difference is $\pi/4$ (corresponding to 3 h in diurnal period) at the coastline and $\pi/2$ at $x = -17$ and 20 cm. This phase difference is consistent with the observed and theoretical results previously published (*e.g.*, Asai and Mitsumoto, 1978).

For a more detailed examination, the LSB shown in the water tank was simulated numerically. The

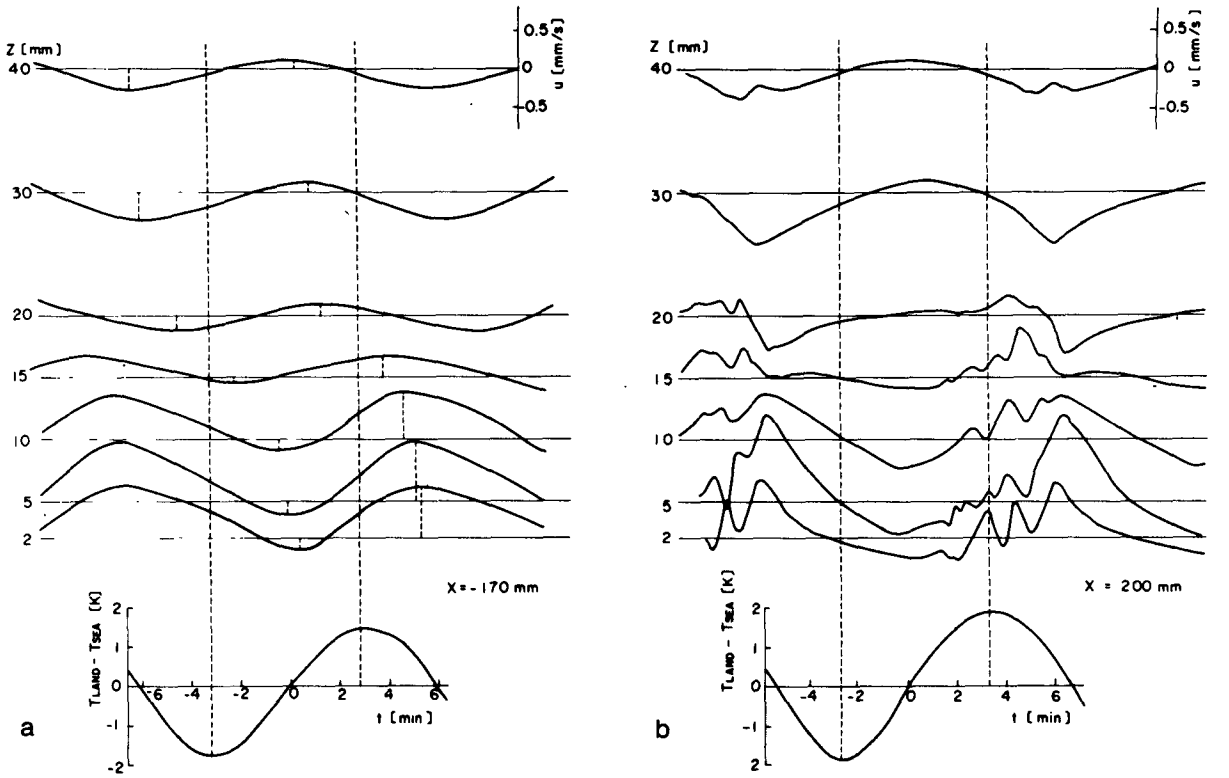

FIG. 4. Horizontal velocity u measured at each level at (a) 0.17 m offshore and (b) 0.20 m inland.

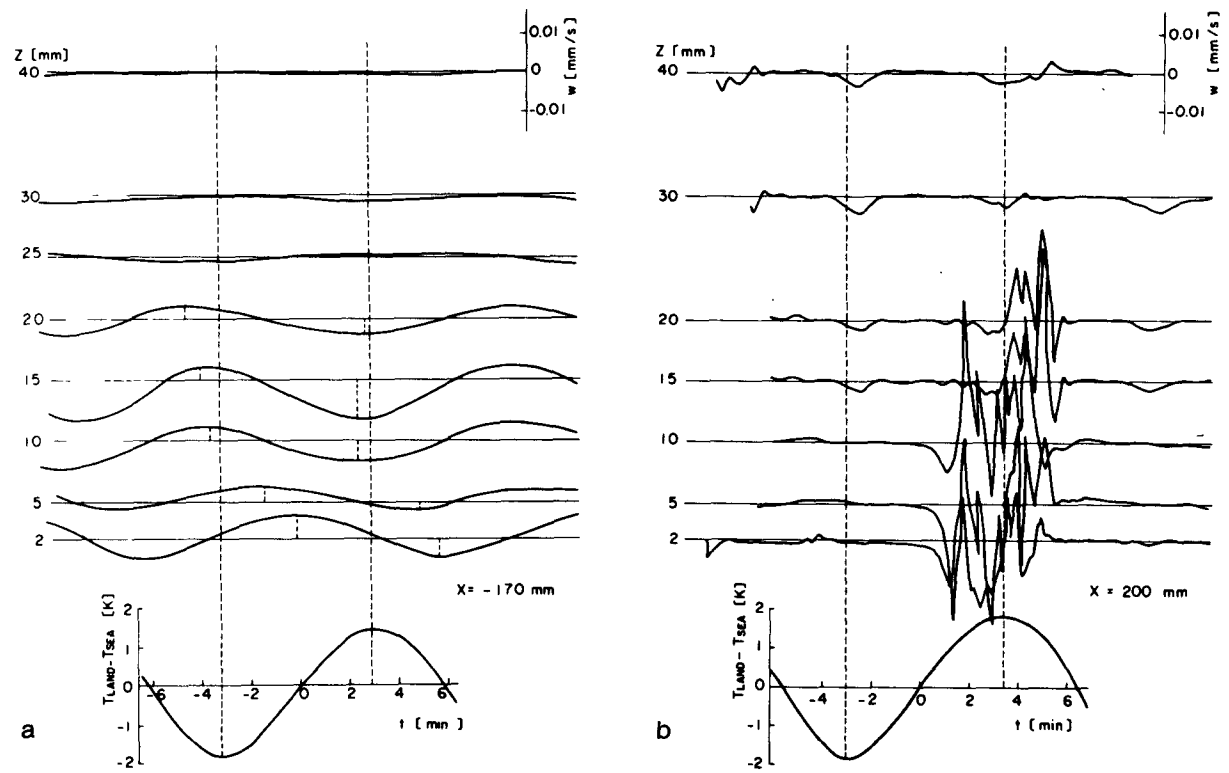

FIG. 5. Vertical velocity w measured at each level at (a) 0.17 m offshore and (b) 0.20 m inland.

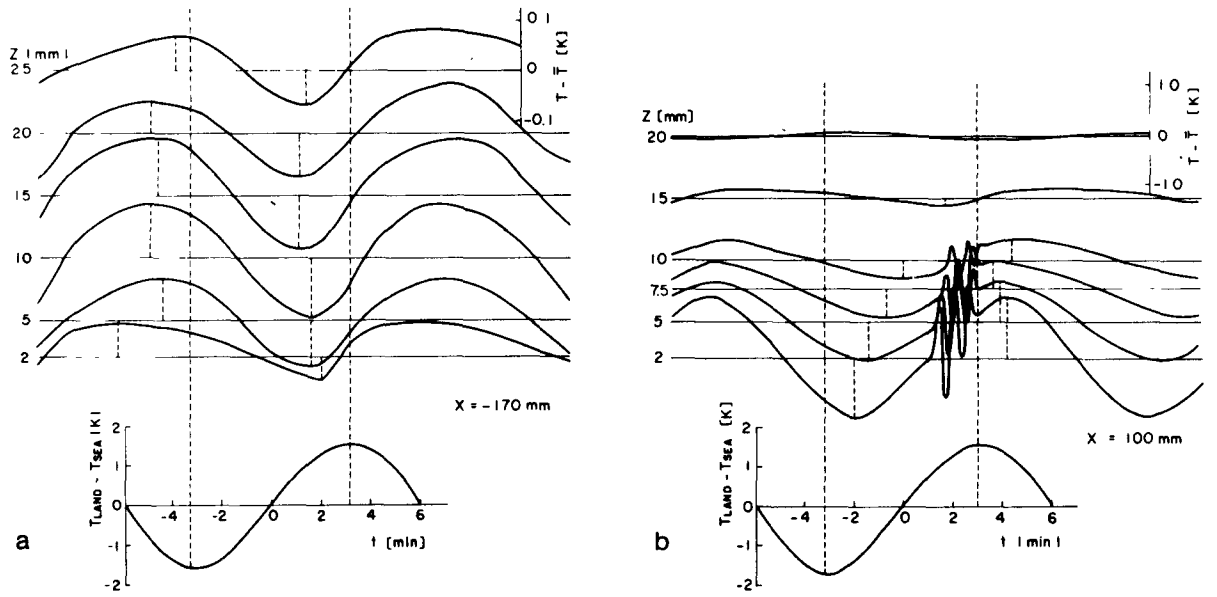

FIG. 6. Temperature T measured at each level at (a) 0.17 m offshore and (b) 0.10 m inland. The base line represents the mean value over a period at each level.

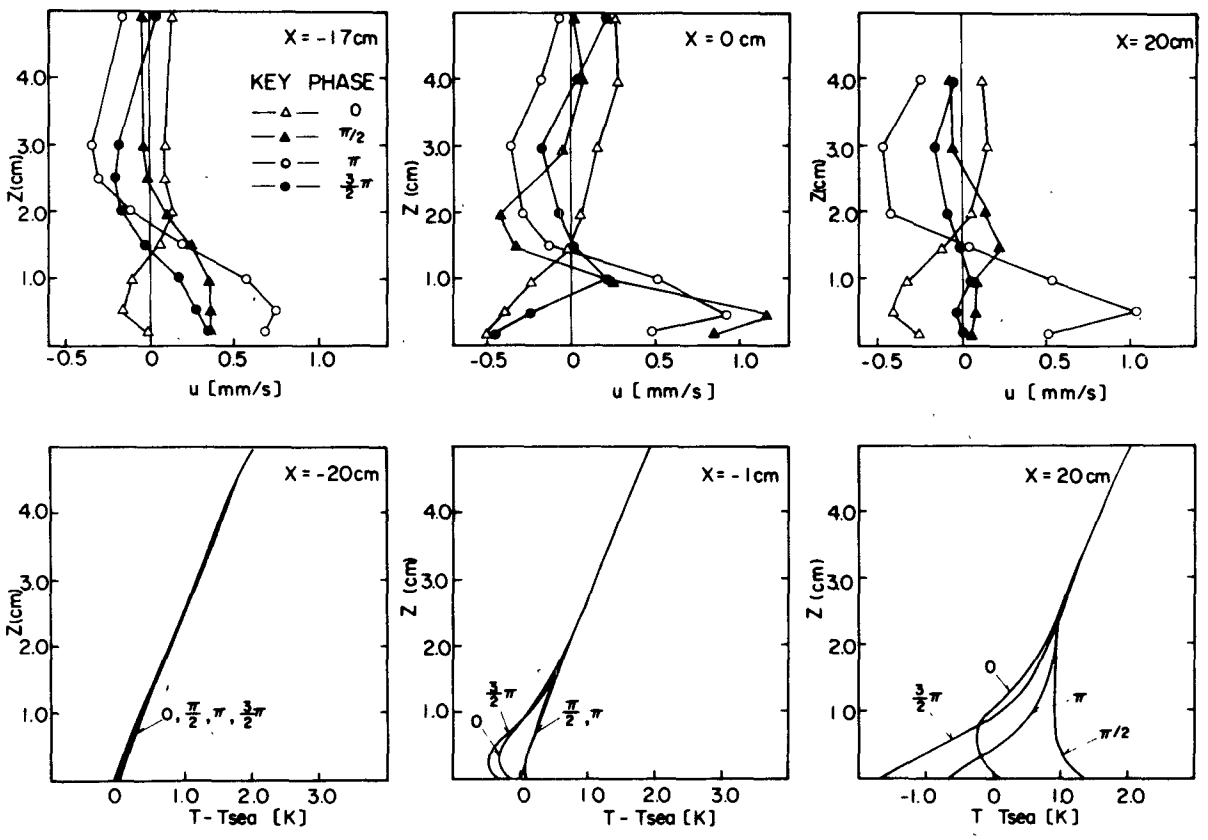

FIG. 7. Vertical profile of horizontal velocity (upper) and of temperature (lower) at the sections above the sea, the coast line, and land. The phase shown in the figure refers to the time variation of T_{LAND}, $\pi/2$ corresponding to the maximum of T_{LAND}, $3\pi/2$ to its minimum.

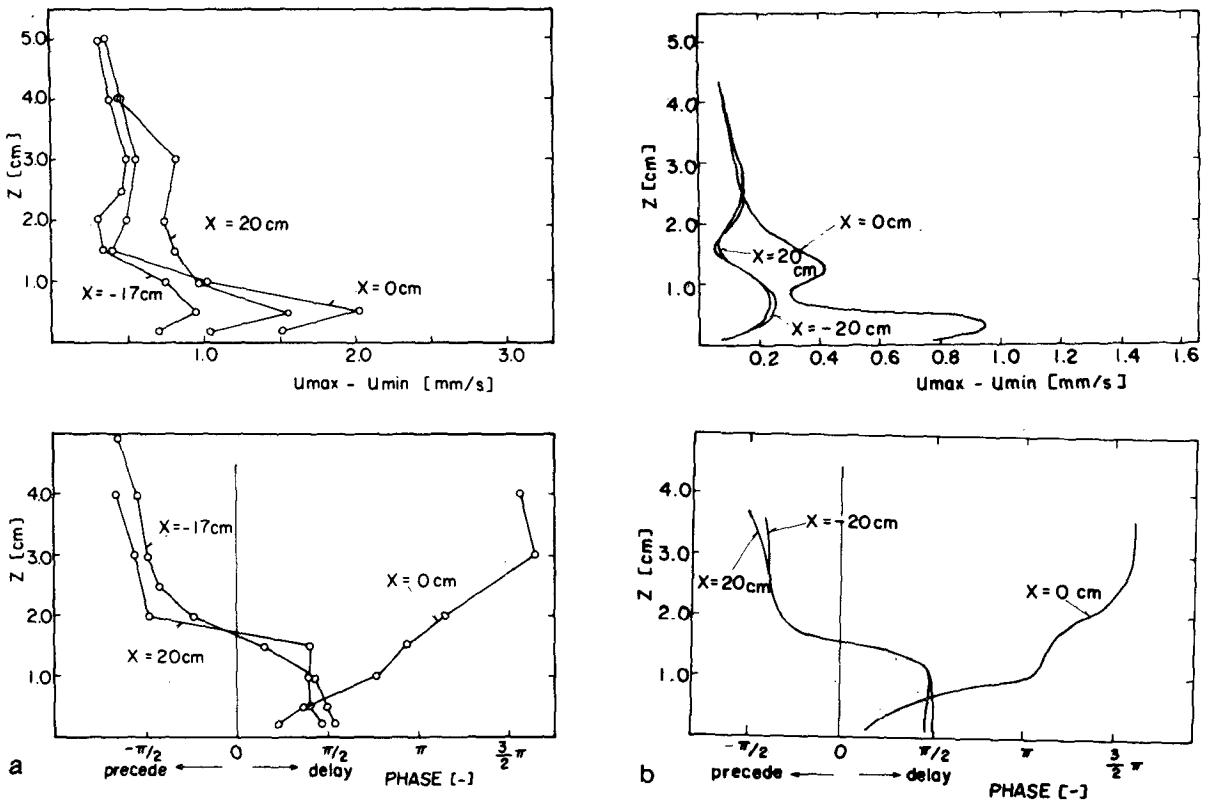

FIG. 8. Vertical profile of amplitude and phase of horizontal velocity u at each section: (a) laboratory experiment and (b) numerical simulation corresponding to the laboratory experiment.

numerical model presented by Asai and Mitsumoto (1978) was used, assuming the physical parameters constant. The results of the amplitude and phase difference are shown in Fig. 8b. The vertical profile of the phase approximately coincides with the results of the laboratory experiment. However, the values of amplitude are too small although the shapes of the vertical distributions are similar. The difference between the numerical and experimental results is attributed to evolution of the cellular convection which is not considered in the numerical simulation.

The singularity of phase behavior above the coastline was discussed by Kimura and Eguchi (1978) based on a linear theory. They showed that the disturbance propagates upward above the coastline because of the character of the heat conduction wave and propagates downward above the land and the sea because the internal gravity wave is dominant there. The result of the present experiment, as well as the numerical results, gives support to this theory.

The horizontal extent of the LSB circulation is shown in Fig. 9. Here, the horizontal velocity at $z = 5$ mm is plotted against distance x from the coastline, since the amplitude of u at this level is greatest. Here u_{max} denotes the maximum sea breeze velocity and u_{min} the maximum land breeze velocity. The sea breeze u_{max} is greatest at $x = 10$ cm, while the absolute value of u_{min} is greatest at the coastline. Both u_{max} and u_{min} rapidly approach zero on the sea side, while they decrease slowly inland. This is attributed to the cellular convection which prevails all over the land. This measurement also confirms that the x length of the test tank is enough so that the fluid motion is not significantly affected by the end walls.

The delay of u_{max} to the maximum of T_{LAND} increases with distance from the coastline. The propagation speed of u_{max} toward both inland and offshore is ~ 3 mm s^{-1}, greater than the speed of sea breeze itself, although it is not evidently determined on the land side more than 30 cm apart from the coastline. The delay of u_{min} (maximum land breeze velocity) relative to the minimum T_{LAND} increases, as in the case of u_{max}, as departing toward the sea from the coastline, its propagation speed again being 3 mm s^{-1}. But the delay of u_{min} is almost constant on the land side. Such a difference in mechanisms of the phase propagation will be discussed in Section 5b.

Fig. 10 is a two-dimensional illustration of the flow pattern at each phase ϕ of the T_{LAND} based on the measurements of u and w (Figs. 4 and 5). The pattern at $\phi = 3\pi/2$ shows the land breeze advancing along the sea surface into a surrounding head wind, the

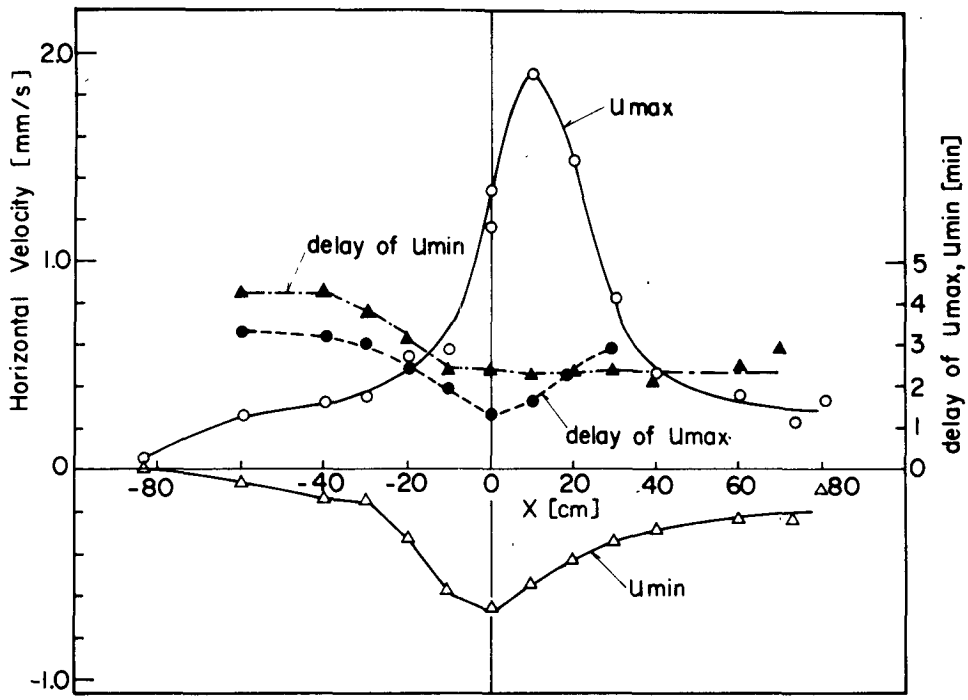

FIG. 9. Horizontal distribution of maximum and minimum u at $z = 5$ mm.

remnant of the sea breeze. A rising flow occurs at the leading edge of the land breeze head. It moves forward far offshore at $\phi = 0$. At $\phi = \pi/2$, where violent cellular convection prevails over the land surface, the sea breeze exists near the coastline, its head having a counterclockwise circulation. At $\phi = \pi$, the sea breeze prevails all over the land and sea surfaces and a strong reverse flow (compensating flow) arises aloft.

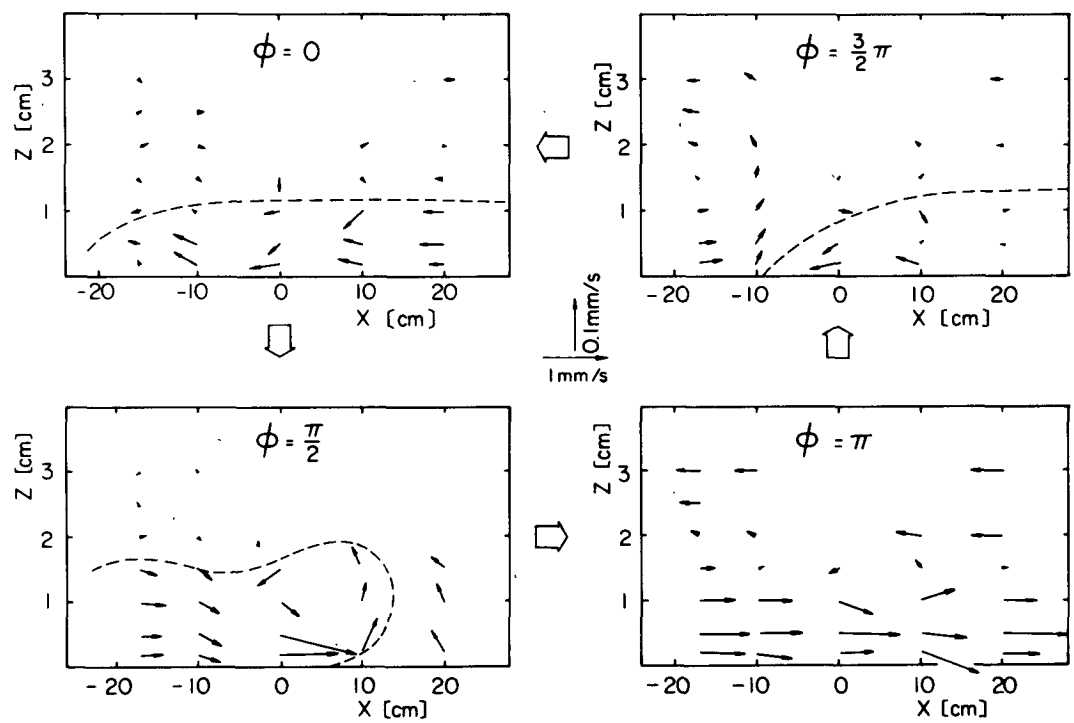

FIG. 10. Two-dimensional distribution of velocity vector at each phase of T_{LAND}. Scale in vertical direction is expanded by eight times more than that in horizontal direction. Ratio of w to u is also expanded by eight times.

5. Discussion

a. Similarity variables of land and sea breeze

Dimensionless external parameters and their effects on the scales and strength of the land and sea breeze circulation can be determined approximately by a linear model (Walsh, 1974; Ueda, 1982).

Let us introduce the following dimensionless variables:

$$\left.\begin{aligned} t^* &= t/\omega, \quad (x^*, z^*) = L(x, z), \quad b^* = b_{0,\max} b \\ (u^*, v^*, w^*) &= (b_{0,\max}/\omega)(u, v, w) \\ p^* &= b_{0,\max} L p \end{aligned}\right\}, \quad (1)$$

where the asterisk denotes dimensional variables, t the time, (u, v, w) the velocity components in the (x, y, z) directions, respectively, p the static pressure, $b = g\beta\theta$, $b_{0,\max}$ the maximum difference of b between the land and sea surfaces, which is also the amplitude of temperature variation at the land surface, g the gravitational acceleration, β the thermal expansion coefficient, θ the deviation of potential temperature from the basic state Θ, ω the angular velocity of temperature variation and L the length scale defined by $(\nu/\omega)^{1/2}$. Here, L, ω^{-1} and $b_{0,\max}$ represent scales of length, time and buoyancy, respectively. Furthermore, $b_{0,\max}$ can be expressed by the combination of ω, L and a dimensionless external parameter determined from the boundary condition of temperature at the land surface, i.e., Grashof number Gr_0 $(=b_{0,\max}/\omega L = g\beta\theta_{0,\max}L^3/\nu^2)$ based on $\theta_{0,\max}$, the maximum temperature difference between land and sea. As seen in Eq. (1), the dimensional velocities are directly proportional to Gr_0.

Assuming that the eddy diffusivities of momentum and heat, ν and κ, are constant and making use of the dimensionless variables, we obtain a linearized set of equations for the two-dimensional land and sea breeze as

$$\frac{\partial u}{\partial t} - (f/\omega)v = -\frac{\partial p}{\partial x} + \nabla^2 u, \quad (2)$$

$$\frac{\partial v}{\partial t} + (f/\omega)u = \nabla^2 v, \quad (3)$$

$$\frac{\partial w}{\partial t} = -\frac{\partial p}{\partial z} + \nabla^2 w + b, \quad (4)$$

$$\frac{\partial b}{\partial t} + \mathrm{Gr}_\Gamma w = \frac{1}{\mathrm{Pr}}\nabla^2 b, \quad (5)$$

$$\frac{\partial u}{\partial x} + \frac{\partial w}{\partial z} = 0, \quad (6)$$

where f is the Coriolis parameter.

We now have three external parameters Gr_Γ $(=g\beta\Gamma L^4/\nu^2$, Γ; the lapse rate $= d\Theta/dz)$, Pr $(=\nu/\kappa)$ and f/ω in addition to Gr_0.

Ueda (1983) solved this set of equations and examined the dependence of the horizontal and vertical scales and strength of the land and sea breeze circulation on these external parameters. They are expressed as

$$\left.\begin{aligned} u_{\mathrm{ref}} &\propto \mathrm{Gr}_\Gamma^{-1/2}\,\mathrm{Pr}^{-2/3} \\ z_{\mathrm{ref}} &\propto \mathrm{Pr}^{-1/4} \\ x_{\mathrm{ref}} &\propto \mathrm{Gr}_\Gamma^{0.387} \end{aligned}\right\}. \quad (7)$$

around a standard condition $\mathrm{Gr}_\Gamma = 18\,500$, $\mathrm{Pr} = 0.83$ and $f/\omega = 1.5$ in the atmosphere.

As seen in Eq. (7), z_{ref} does not depend on Gr_Γ and x_{ref} does not depend on Pr. The effect of f/ω is negligible, except for the velocity component parallel to the coastline, not discussed here. These relations are found to be valid over the ranges of Gr_Γ and Pr more than two orders of magnitude and suggested that new dimensionless variables u^+ $(=u\,\mathrm{Gr}_\Gamma^{1/2}\,\mathrm{Pr}^{2/3})$, z^+ $(=z\,\mathrm{Pr}^{1/4})$ and x^+ $(=x\,\mathrm{Gr}_\Gamma^{-0.387})$ are universal similarity variables for the land and sea breeze.

Introduction of these variables makes a comparison of the land and sea breezes in atmospheric and laboratory scales possible. In Table 1, the values obtained from the present experiment are compared with plausible values in field measurements reported hitherto. Gr_Γ, Gr_0 and f/ω obtained in the laboratory are far smaller than those in the atmosphere. However, the Gr_0 value of the laboratory experiment was large enough to make the flow unstable, i.e., to cause cellular convection over land in the morning calm.

The ranges of Gr_Γ and Gr_0 in this laboratory experiment are limited, but the present experiment gives reasonable values for the similarity variables x^+, z^+ and u^+. Therefore, it can be said that the present experiment successfully simulated the land and sea breeze which takes place in the atmosphere.

b. Physical mechanisms constituting the LSB

As pointed out in Section 4a, the land and sea breeze is composed of several small scale motions, such as cellular convection, longitudinal vortex motion and gravity current. Physical mechanisms which contribute to the land breeze and sea breeze are different from each other. These motions are rather small in scale compared with the land and sea breeze circulation as a whole, but contribute substantially to the overall fluid motion of the land and sea breeze and cause the difference in flow patterns between night and day. Since these mechanisms have not been discussed in detail in relation to the LSB, further discussion on each of them will be given below.

1) CELLULAR CONVECTION

Cellular convection over land is caused by unsteady heating from below. Generally, when a stably

TABLE 1. Comparison of non-dimensional values between field measurement and laboratory experiment.

	Field observation			Laboratory experiment		
	$\omega = 7.27 \times 10^{-5}$ (rad s^{-1}) $L = 262$ m $\nu = 10$ m^2 s^{-1} $Gr_\Gamma = 19000$ $\Gamma = 3 \times 10^{-3}$ K m^{-1} Pr = 1.0 $f/\omega = 1.5$ $Gr_0 = 85300$			$\omega = 1.75 \times 10^{-2}$ (rad s^{-1}) $L = 7.56$ mm $\nu = 1$ mm^2 s^{-1} $Gr_\Gamma = 672$ $\Gamma = 0.1$ K mm^{-1} Pr = 6.8 $f/\omega = 6.23 \times 10^{-4}$ $Gr_0 = 1330$		
Horizontal scale	$x^* = 45$ km*	$x = 171.7$	$x^+ = 3.79$	$x^* = 300$ mm*	$x = 39.7$	$x^+ = 3.20$
Vertical scale (thickness of sea breeze layer)	$z^* = 700$ m	$z = 2.67$	$z^+ = 2.67$	$z^* = 20$ mm	$z = 2.64$	$z^+ = 4.26$
Velocity scale (maximum wind speed)	$u^* = 5$ m s^{-1}	$u = 2.17 \times 10^{-3}$	$u^+ = 0.30$	$u^* = 1.0$ mm s^{-1}	$u = 5.67 \times 10^{-3}$	$u^+ = 0.528$

* The horizontal scale x^* is defined as the range in which the amplitude of u is greater than 50% of u_{max}. This value in field measurements is supported by numerical results (*e.g.*, Yoshikado and Asai, 1972; Asai and Mitsumoto, 1978).

stratified infinite fluid layer at rest is heated periodically from below and if the Grashof number Gr_0 is greater than a certain critical value, a flow instability occurs in the form of a Bénard-type disturbance at the moment when the thickness of the unstable layer exceeds a certan critical value. Thus, for evolution of the cellular convection, a certain time lag is necessary after heating starts.

Fig. 11 shows the plan views of the cellular convection: (a) when the convection commenced, (b) about 0.5 min later. The mean diameter of each cell in Fig. 11a is ~2 cm, the same as its height. With the evolution of the convection, the initial cells merge into larger cells. This cellular convection forms a mixed layer with a uniform thickness all over the land surface.

The convective cells in the atmosphere were observed in optically clear air by Konrad (1970) using *S*-band radar. Convective cells occurred following the destruction of the surface stable layer. The cells first appeared ring-shaped, as small as ~100–200 m in diameter, and they gradually grew both in height and diameter, merging into larger cells. The radar echo patterns obtained in the atmosphere and the visualized cellular patterns obtained in the present experiment seem to be quite similar, at least in their shapes.

The cellular convection has a certain significance with respect to transport of pollutants emitted from the ground. As seen in Photo 2 of Fig. 2, the convection carries upward the pollutant which has been hovering near the land surface. It also transports pollutants from elevated plumes downward to the surface as well. Pollutants at the top of the mixed layer, together with pollutants lifted up by the sea breeze front, are later transported seaward by the compensating flow. Thus, a high concentration layer just above the sea breeze layer is created and penetrates toward the sea side. This is clearly seen in all photographs in Fig. 2 as the layered structure in the background.

2) LONGITUDINAL VORTEX ROWS

When the sea breeze intrudes over the land after the convective cells have merged into larger ones and attenuated, longitudinal vortex rows arise, the plan

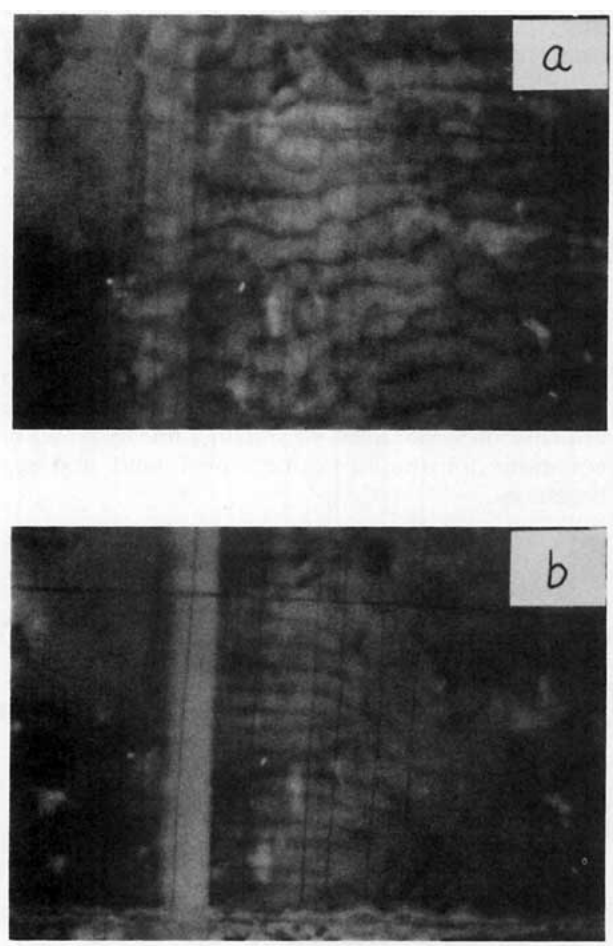

FIG. 11. Plan view of the cellular convection and the following longitudinal vortex rows: (a) when convection occurred and (b) 30 s afterward.

views of which are shown in Figs. 3b and 11b. The appearance of longitudinal vortices has been generally recognized as a phenomenon which occurs when a colder fluid moves horizontally over a heated surface and when the Grashof number is larger than a critical value (*e.g.*, Fukui *et al.*, 1982). The vortex width is almost equal to the vortex height. In the present case, it coincides with thickness of the sea breeze layer. In addition, it is surprising that the vortex width is uniform from the edge (coastline), as shown in Fig. 11b. Inland, ahead of the sea breeze front the mixed layer generated by the cellular convection still exists.

3) GRAVITY CURRENTS

Gravity current is defined as the flow of a heavy fluid under a lighter one. It is characterized by strong swirling and mixing with the surrounding fluid at its head, and by updraft at the leading edge of this head. Detailed dynamics of the gravity current were made clear by Simpson and Britter (1979, 1980).

Both the sea and land breezes are identified as gravity currents. However, there is a clear difference between them. The sea breeze advances into the mixed layer, accompanied by longitudinal vortex motions over the land surface. The mixed layer is generated by cellular convection, and there is no mean horizontal flow in it. The land breeze, on the other hand, moves forward against a head wind which is stably stratified. Thus, the land breeze head has a flattened shape, its thickness in the laboratory being less than 5 mm, and penetrates underneath the surrounding fluid, reducing the strength of the updraft at the leading edge.

Such different features between sea and land breeze fronts are schematically depicted in Fig. 12.

As mentioned in Section 4c, another difference between the sea and land breezes arises in the phase propagation (Fig. 9). In the land breeze case, due to unsteady cooling from below, a stably stratified fluid layer is formed uniformly over the land surface and grows in thickness. When it intrudes over the sea surface as a gravity current, the flow following the land breeze head is regarded as a horizontal movement of the cold fluid layer like a solid plate, because the fluid layer is stably stratified, and accordingly, the entrainment from the upper layer is insignificant. Thus, the phase of $u_{\min}$ is almost constant on the land side, *i.e.*, the maximum land breeze occurs at the same instant all over the land surface (Fig. 12).

In contrast to this, the phase delay of the maximum sea breeze $u_{\max}$ to the maximum of T_{LAND} increases with distance from the coastline toward both the land and the sea. This phase propagation may be explained as an expansion of the circulating zone generated initially near the coastline in the same manner as those shown in linear theories on LSB (*e.g.*, Kimura and Eguchi, 1978). Since the lower layer over the sea is always stratified with the basic lapse rate (Fig. 7) and is not accompanied by the unsteady cooling seen over the land in the land breeze case, the fluid following the sea breeze head is supplied from the upper layer as well as from offshore. Thus, the overall feature of the flow pattern in the initial stage of the sea breeze phase appears as a closed circulation which expands toward both the land and sea sides.

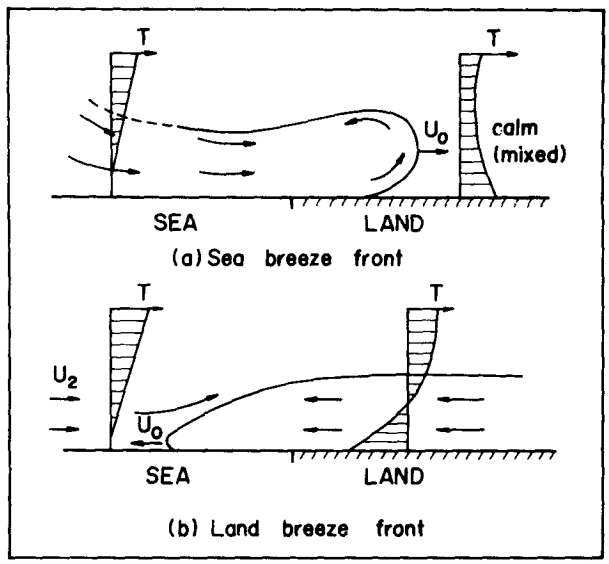

FIG. 12. Sketch of land and sea breeze fronts. Vertical profile of the temperature is shown schematically at each section. Advance speed of the leading edge is U_0, and U_2 is speed of "head wind."

The advance speed U_0 of the land breeze head was determined from continuous photographs of the front. It was found to be constant at 0.676 mm s^{-1} in the region $x < -50$ mm. This advance speed is in good agreement with the value (0.61 mm s^{-1}) calculated by the empirical relation $U_0 = 0.7|u_{\min}| + 0.3U_2$, where U_2 is the speed of the surrounding flow against the gravity current head, which is 0.4 mm s^{-1} in the present case. This empirical relation was obtained by Goff (1976) who observed sea breeze and thunderstorm outflow fronts and was confirmed by Simpson and Britter (1980) in a laboratory experiment.

On the other hand, the advance speed U_0 of the sea breeze head is 1.36 mm s^{-1} in the region $x > 50$ mm. The advance speed multiplied by 1.5 is equal to $u_{\max}$, the maximum of sea breeze speed (2.0 mm s^{-1}). This is again in agreement with the aforementioned relation or $U_0 = (2/3)|u_{\max}|$ proposed by Clarke (1961). The phase speed of $u_{\max}$ was 3 mm s^{-1}, far greater than U_0 or $u_{\max}$ itself.

6. Conclusions

The land and sea breeze (LSB) circulation was investigated in a laboratory experiment using a tem-

perature-controlled water tank. Similarity with that in the atmosphere was confirmed by a linear model of the LSB. The laboratory experiment elucidated the physical mechanisms which constitute the LSB and their contribution to the overall features of the LSB.

In the morning calm, Bénard-type cellular convection breaks out all over the land surface due to the unsteady heating from below. This forms a mixed layer with uniform thickness inland. After the convection cells have merged into larger ones and subsequently weakened, the sea breeze appears. When it advances over land and is heated from below, longitudinal vortex rows are formed throughout the sea breeze layer.

Both the sea and land breezes are gravity currents. However, the land breeze advances against a head wind in stably stratified surroundings and so, the land breeze head has a flattened shape and penetrates underneath the surrounding fluid, the updraft at the leading edge not being so strong as in the sea breeze. On the other hand, the sea breeze advances into the mixed layer which had been generated by cellular convection and is accompanied by a strong updraft at the leading edge of the head. It looks like the extension of the circulation zone generated initially above the coastline.

Thus, it was clarified that the overall feature of the LSB is the combination of closed circulation caused by the periodically changing temperature difference between land and sea and of the small-scale motions induced by the periodic variation of the land surface temperature itself. The latter contributes to making the LSB asymmetrical. Small-scale motions, such as cellular convection, longitudinal vortex and gravity current, are important not only for the LSB itself but also for the transport of pollutants in it.

Acknowledgments. The authors would like to express their deep gratitude to Prof. T. Asai and Prof. R. Kimura, Ocean Research Institute, University of Tokyo, who read the manuscript carefully and gave them valuable comments to improve the paper. They also thank Mr. T. Shibata, Okayama University and Mr. K. Chiba, Entoku Elementary School, Nagano, and Miss E. Kimura for their help in the laboratory experiment and data processing. This study was made as a Research Project in the National Institute for Environmental Studies and was also financially supported by the Fund for the Scientific Research of the Ministry of Education, Japan.

REFERENCES

Anthes, R. A., and T. T. Warner, 1978: Development of hydrodynamic models suitable for air pollution and other mesometeorological studies. *Mon. Wea. Rev.*, **106,** 1045–1077.

Asai, T., and S. Mitsumoto, 1978: Effects of an inclined land surface on the land and sea breeze circulation: A numerical experiment. *J. Meteor. Soc. Japan,* **56,** 559–570.

Clarke, R. H., 1961: Mesostructure of dry cold fronts over featureless terrain. *J. Meteor.*, **18,** 715–735.

Defant, F., 1951: Local winds. *Compendium of Meteorology,* Amer. Meteor. Soc., 655–672.

Estoque, M. A., 1961: A theoretical investigation of the sea breeze. *Quart. J. Roy. Meteor. Soc.*, **87,** 136–146.

——, 1962: The sea breeze as a function of the prevailing synoptic situation. *J. Atmos. Sci.*, **19,** 244–250.

Fukui, K., M. Nakajima and H. Ueda, 1982: Longitudinal vortex and its effects on the transport processes in combined free and forced convection between horizontal and inclined parallel plates. *Int. J. Heat Mass Transfer,* **26,** 109–120.

Goff, R. C., 1976: Thunderstorm-outflow kinematics and dynamics. NOAA. Tech. Memo. ERL NSSL-75, 63 pp.

Haurwitz, B., 1941: *Dynamic Meteorology.* McGraw-Hill, 139–140.

——, 1947: Comments on the sea-breeze circulation. *J. Meteor.*, **4,** 1–8.

Jeffreys, H., 1922: On the dynamics of wind., *Quart. J. Roy. Meteor. Soc.*, **48,** 29–46.

Keen, C. S., and W. A. Lyons, 1978: Lake/land breeze circulation on the western shore of Lake Michigan. *J. Appl. Meteor.*, **17,** 1843–1855.

Kikuchi, Y., S., Arakawa, F. Kimura, K. Shirasaki and Y. Nagano, 1981: Numerical study on the effects of mountains on the land and sea breeze circulation in the Kanto district. *J. Meteor. Soc. Japan,* **59,** 723–738.

Kimura, R., and T. Eguchi, 1978: On the dynamical process of sea- and land-breeze circulation. *J. Meteor. Soc. Japan,* **56,** 67–85.

Kondo, H., and K. Gambo, 1979: The effects of the mixing layer on the sea breeze circulation and the diffusion of pollutants associated with land-sea breezes. *J. Meteor. Soc. Japan,* **57,** 560–575.

Konrad, T. G., 1970: The dynamics of the convective process in clear air as seen by radar. *J. Atmos. Sci.*, **27,** 1138–1147.

Lyons, W. A., and L. E. Olsson, 1973: Detailed mesometeorological studies of air pollution dispersion in the Chicago lake breeze. *Mon. Wea. Rev.*, **101,** 387–403.

Mahrer, Y., and R. A. Pielke, 1977: The effects of topography on sea and land breezes in a two-dimensional numerical model. *Mon. Wea. Rev.*, **105,** 1151–1162.

McPherson, R. D., 1970: A numerical study of the effect of a coast irregularity on the sea breeze. *J. Appl. Meteor.*, **9,** 767–777.

Ozoe, H., T. Shibata, H. Sayama and H. Ueda, 1983: Characteristics of air pollution in the presence of land and sea breeze—A numerical experiment. *Atmos. Environ.* **17,** 35–42.

Simpson, J. E., and R. E. Britter, 1979: The dynamics of a head of a gravity current advancing over a horizontal surface. *J. Fluid Mech.*, **94,** 477–495.

——, and ——, 1980: A laboratory model of an atmospheric mesofront. *Quart. J. Roy. Meteor. Soc.*, **106,** 485–500.

Ueda, H., S. Mitsumoto and S. Komori, 1981: Buoyancy effects on the turbulent transport processes in the lower atmosphere. *Quart. J. Roy. Meteor. Soc.*, **107,** 561–578.

——, 1983: Effects of external parameters on the flow field in the coastal region—A linear model. *J. Appl. Meteor.* **22,** 312–321.

Walsh, J. E., 1974: Sea breeze theory and application. *J. Atmos. Sci.*, **31,** 2012–2026.

Wexler, R., 1946: Theory and observation of land and sea breezes. *Bull. Amer. Meteor. Soc.*, **27,** 272–287.

Yoshikado, H., and T. Asai, 1972: A numerical experiment of effects of turbulent transfer processes on the land and sea breeze. *Contrib. Geophys. Inst., Kyoto Univ.*, **12,** 33–48.